Coulomb dynamical polarization potential and the electric dipole polarizability for weakly bound and neutron-rich light nuclei

H. M. Maridi [*] and K. Rusek [†]
Heavy Ion Laboratory, University of Warsaw, ulica Pasteura 5a, 02-093, Warsaw, Poland

N. Keeley [‡]
National Centre for Nuclear Research, ulica Andrzeja Sołtana 7, 05-400 Otwock, Poland

(Received 12 April 2021; revised 6 July 2021; accepted 11 August 2021; published 24 August 2021)

In this paper, we present a method to determine the dipole polarizability of light exotic nuclei with a two-body deuteronlike cluster structure. Using the adiabatic approximation, we solve the Schrödinger equation for the internal motion of the exotic projectile incident on a heavy target nucleus and express the resulting Coulomb dynamical polarization potential (CDPP) in terms of regular and irregular Coulomb functions. We then obtain a new expression for the dipole polarizability (α_0) by equating the real part of this CDPP to the classical expression for the polarization potential. The α_0 values for many weakly bound light nuclei are calculated and where values are available were found to be in good agreement with those obtained in previous studies using various other methods.

DOI: 10.1103/PhysRevC.104.024614

I. INTRODUCTION

When two nuclei interact at energies below the Coulomb barrier the deviation from Rutherford scattering may be represented by a short-range nuclear potential. However, at low energies the lighter colliding partner—usually the projectile—may become polarized by the electric field of the heavier, thus distorting its charge distribution and inducing an additional interaction which influences the elastic scattering. This additional interaction is often referred to as the Coulomb dynamical polarization potential (CDPP). If the projectile is weakly bound this polarization effect may become large, giving rise to a strong Coulomb dipole excitation mode. In the case of halo nuclei where the breakup threshold energy is less than 1 MeV, dipole excitation to the low-lying continuum can be particularly important, see, for example, Ref. [1].

A weakly bound neutron-rich nucleus will be easily distorted if it moves in an electric field where the valence neutron(s) moves in the opposite direction to the charged core. This phenomenon is known as the dipole polarizability [2] (although it is not restricted to nuclei of this class). Usually, the nuclear dipole polarizability is neglected for stable nuclei where the $B(E1)$ strength distribution peaks at relatively high excitation energies. However, a weakly bound projectile with low breakup threshold can break up and become polarized due to a strong external Coulomb field with significant probability, leading to a reduction in the elastic-scattering cross section. This dipole polarization can be represented by the electric dipole polarizability, α_0, which may be calculated from first principles or derived from the $B(E1)$ strength distribution as follows:

$$\alpha_0 = \frac{8\pi}{9}\int \frac{1}{\varepsilon}\frac{dB(E1,\varepsilon)}{d\varepsilon}d\varepsilon. \tag{1}$$

Recently, a method has been developed to extract such $B(E1)$ distributions for weakly bound nuclei from Coulomb dissociation data using continuum-discretized coupled channels (CDCC) calculations [3].

If the incident energy is sufficiently low such that nuclear effects may be neglected (and any Coulomb excitation of the heavy target nucleus is small enough to be ignored), i.e., the Sommerfeld parameter $\eta \gg 1$, the classical approximation is valid, and the following expression for the purely real classical CDPP in terms of the dipole polarizability α_0 is obtained [4]

$$\delta V_R = -\frac{1}{2}\alpha_0\frac{Z_T^2 e^2}{R^4}. \tag{2}$$

Under these conditions the dipole polarizability may be extracted from the measured elastic-scattering angular distribution by adding the term (2) to the usual diagonal Coulomb potential and adjusting the value of α_0 to fit the small deviation from Rutherford scattering [5].

In recent years this approach has been extended to include breakup of a weakly bound deuteronlike projectile in addition to the polarization induced by the Coulomb field of a heavy target nucleus, for example, the work of Borowska *et al.* [6] which uses a semiclassical adiabatic formalism. The internal motion of the valence neutrons is treated adiabatically, and the projectile as a whole is assumed to follow a classical Rutherford trajectory. In order to obtain an analytic expression

[*]Permanent address: Department of Physics, Faculty of Applied Science, Taiz University, Taiz, Yemen; hmaridi@slcj.uw.edu.pl
[†]rusek@slcj.uw.edu.pl
[‡]nicholas.keeley@ncbj.gov.pl

for the CDPP a quasiclassical approach is additionally applied to the internal motion of the projectile, resulting in a complex CDPP, the imaginary part representing the effects of breakup. In this adiabatic approximation, the relative motion is slow compared with the time of the excitation $\hbar/E_x$, where E_x is the excitation energy, and the resulting CDPP is local and independent of the scattering energy [7].

The CDPP may be extracted from CDCC calculations by means of the trivially equivalent method [8], for example, and the so-called trivially equivalent local potential (TELP) can represent the dynamical effect well for scattering from heavy targets. Such CDCC calculations can be time consuming and difficult to perform, however, so that alternative means of calculating the CDPP, such as that of Borowska *et al.* [6] which can be used to describe coupling to large sets of states, such as the continuum of breakup states, can be useful tools for the planning and interpretation of experiments. The large dipole transition strength close to the breakup threshold in halo nuclei [9–11] often leads to significant coupling effects on the elastic-scattering angular distribution, particularly in the case of neutron halo nuclei. In addition, most Coulomb-excitation experiments can extract information on the electromagnetic properties of nuclear transitions with relevance to nuclear structure as well as nuclear astrophysics, and Coulomb dissociation can be used to determine the absolute astrophysical $S(E)$ factor for radiative capture reactions $b(x,\gamma)a$ by studying the reverse photodisintegration process where the Coulomb field of a heavy target nucleus is used as a source of virtual photons [12]. Thus, a means of estimating the dipole polarizability α_0 for different possible configurations of such nuclei would also be of value.

In the present paper we derive a new expression for the CDPP of a weakly bound projectile with a two-body deuteron-like cluster structure moving in the strong Coulomb field of a heavy target. By equating the real part of this complex CDPP with the purely real classical expression we present a new method to evaluate the dipole polarizability α_0. Values of α_0 are obtained for many light exotic nuclei and compared with previous determinations using other methods where available. The sensitivity of α_0 to the separation energy is also investigated.

II. THEORY

We follow the procedure of Borowska *et al.* [6] up to and including their Eq. (15), our Eq. (32). We differ in our subsequent handling of the Eq. (32), which must be solved to obtain the CDPP. We do not approximate the Coulomb functions as in Borowska *et al.* where the WKB expressions are used for these quantities.

A. Derivation of the Coulomb polarization potential

Let us consider the scattering problem of a weakly bound projectile (P) moving in the Coulomb field of a heavy target (T) with charge Z_T and mass m_T (see Fig. 1). The projectile has mass m_p and is considered to be a two-body composite object, made up of a charged core (c) (with mass m_c and charge $Z_c = Z_p$) and valence neutron(s) (v) with mass $m_v = nm_n$ (where n is the number of valence neutrons and m_n is the mass of the neutron). In this paper we confine our attention to systems where the valence particle is a neutron or cluster of neutrons in order to avoid the complications associated with the Coulomb interaction between the valence particle and the core and the valence particle and the target for the case of charged valence clusters. The internal structures of the core of the projectile and the target nucleus are not taken into account and their excitations are neglected.

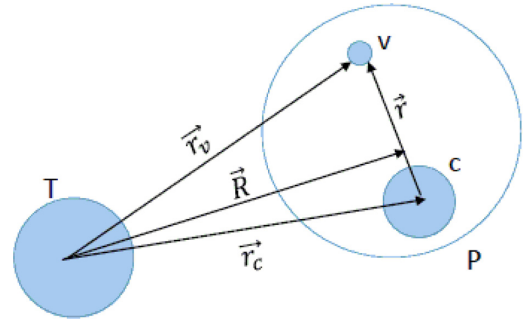

FIG. 1. Coordinates describing the elastic scattering of a projectile (P) in the Coulomb field of a target (T). The weakly bound projectile is considered to have a two-body cluster structure with a charged core (C) and weakly bound neutron(s) (v). See text for further details.

The total system is described by a position vector $\mathbf{R}$ which represents the coordinate of the projectile center-of-mass relative to the target with a system reduced mass of $\mu = m_p m_T/(m_p + m_T) \approx m_p$ and a kinetic-energy operator $T_{\mathbf{R}} = -\hbar^2\Delta_{\mathbf{R}}/2\mu$; $\mathbf{r}_c$ and $\mathbf{r}_v$ are the position vectors of the two projectile clusters [charged core and valence neutron(s)], respectively. The internal system of the projectile is described by a position vector $\mathbf{r}$ representing the relative coordinate of the valence neutron(s) with respect to the core with a kinetic-energy operator $T_{\mathbf{r}} = -\hbar^2\Delta_{\mathbf{r}}/2\mu_p$. The coordinates may then be written as

$$\mathbf{r} = \mathbf{r}_v - \mathbf{r}_c, \quad m_p\mathbf{R} = m_v\mathbf{r}_v + m_c\mathbf{r}_c, \tag{3}$$

and using the projectile reduced mass $\mu_p = m_c m_v/m_p$ in Eq. (3) we get

$$\mathbf{r}_c = \mathbf{R} - \frac{\mu_p}{m_c}\mathbf{r}. \tag{4}$$

The motion of the weakly bound projectile with wave-function $\Psi(\mathbf{r},\mathbf{R})$ in the nuclear and Coulomb fields of the heavy target can be described by the Schrödinger equation,

$$H\Psi(\mathbf{r},\mathbf{R}) = E\Psi(\mathbf{r},\mathbf{R}), \tag{5}$$

where the total energy $E = E_p + \varepsilon_0$ is the sum of the (asymptotic) projectile kinetic-energy E_p and the binding energy ε_0, the separation energy of the valence neutron(s) from the projectile. The Hamiltonian of the system is given by

$$H = T_{\mathbf{R}} + T_{\mathbf{r}} + V_C(\mathbf{r}_c) + V_{vc}(r), \tag{6}$$

where V_C is the Coulomb potential and $V_{vc}(r)$ is the nuclear potential of the weakly bound projectile neutron(s) relative to the projectile core.

The Coulomb potential between the charged projectile core and the target $V_C(\mathbf{r}_c)$ can be considered to consist of two parts: one for the Coulomb scattering of the projectile in the field of the heavy target $V_C(\mathbf{R})$ and a second part $\Delta V_C(\mathbf{r}, \mathbf{R})$, which describes deviations from pure Coulomb scattering due to the internal structure of the projectile (i.e., Coulomb excitation) as follows:

$$V_C(\mathbf{r}_c) = V_C(\mathbf{R}) - \Delta V_C(\mathbf{r}, \mathbf{R}), \tag{7}$$

and the total Hamiltonian then becomes

$$\begin{aligned} H &= T_{\mathbf{R}} + T_{\mathbf{r}} + V_C(\mathbf{R}) - \Delta V_C(\mathbf{r}, \mathbf{R}) + V_{vc}(r) \\ &= H_0 - \Delta V_C(\mathbf{r}, \mathbf{R}). \end{aligned} \tag{8}$$

Since the internal motion of the weakly bound neutron(s) is faster than the total projectile motion in the target field we can use the adiabatic Born-Oppenheimer approximation for the wave function as in Refs. [13–15],

$$\Psi(\mathbf{r}, \mathbf{R}) = \chi(\mathbf{R})\phi(\mathbf{r}, \mathbf{R}), \tag{9}$$

where $\chi(\mathbf{R})$ refers to the wave function of the center of mass and $\phi(\mathbf{r}, \mathbf{R})$ refers to that of the relative motion of the projectile.

Using separation of variables, the Schrödinger equation (5) can be written as [6]

$$[T_{\mathbf{R}} + V_C(\mathbf{R})]\chi(\mathbf{R}) = \{E - [\varepsilon_0 + \delta V(R)]\}\chi(\mathbf{R}), \tag{10}$$

$$[T_{\mathbf{r}} - \Delta V_C(\mathbf{r}, \mathbf{R}) + V_{vc}(r)]\phi(\mathbf{r}, \mathbf{R}) = [\varepsilon_0 + \delta V(R)]\phi(\mathbf{r}, \mathbf{R}). \tag{11}$$

In addition to polarization of the mass and charge distributions of the weakly bound projectile, the Coulomb field of the target may also lead to its breakup into the charged core and the weakly bound neutron(s). To take account of these effects the binding energy of the valence neutron(s) to the charged core of the projectile is modified by the addition of a small complex potential $\delta V(R)$ [6,14,16], often referred to as the CDPP. It parametrically depends on the center-of-mass coordinate R due to the fact that the projectile internal motion is fast compared with its motion through the Coulomb field of the target. In addition, the projectile breakup is determined by the imaginary part of the CDPP. The internal wave function describing the interaction between the core and the valence neutron(s) is usually given as [14,17]

$$\phi_0(\mathbf{r}) = \sqrt{\frac{\alpha}{2\pi}}\frac{e^{-\alpha r}}{r}, \tag{12}$$

where

$$\alpha = \sqrt{\frac{-2\mu_p\varepsilon_0}{\hbar^2}}. \tag{13}$$

In principle, the nucleons inside the core have some spatial distribution, and the interaction between the nucleons also has a finite range. At low energies, the range of the potential between the core and the valence neutrons is much smaller than the wavelength of the projectile and can be neglected, so we can make use of the zero-range approximation [18]. This is suitable for systems involving light-ion projectiles with small threshold energies [19]. In addition, making the zero-range approximation enables Eq. (11) to be solved. Before doing so we test the effect of using a finite-range potential, for example, the Hulthén interaction with a range of $1/\mu_0$ [20],

$$V_{vc}(r) = \frac{-\hbar^2}{2\mu_p}\mu_0(\mu_0 + \alpha)\frac{e^{-\mu_0 r}}{1 - e^{-\mu_0 r}}, \tag{14}$$

which corresponds to the following form for the exact wave function of the projectile,

$$\phi_0(\mathbf{r}) = \frac{1}{\sqrt{4\pi}}\sqrt{\frac{2\alpha(\mu_0 + \alpha)(\mu_0 + 2\alpha)}{\mu_0^2}}\frac{e^{-\alpha r}}{r}(1 - e^{-\mu_0 r}), \tag{15}$$

which tends to (12) as $\mu_0 \to \infty$, and we obtain the form factor as [21]

$$\begin{aligned} F\left(q_v^2\right) &= \left\langle \phi_0^v(\mathbf{r}) \middle| V_{vc}(r) \middle| \phi_0(\mathbf{r}) \right\rangle \\ &= -\frac{V_0}{\sqrt{4\pi}}\frac{(\mu_0 + \alpha)^{1/2}(\mu_0 + 2\alpha)^{3/2}}{(\mu_0 + \alpha)^2 + q_v^2} \end{aligned} \tag{16}$$

where $V_0 = \sqrt{8\pi\alpha}\hbar^2/2\mu_p$, $\phi_0^v = e^{-iq_v r_v}$ denote the valence plane wave [21]. For low projectile energies where q_v is small, and at small threshold energies (small α) we have $F(q_v^2) \approx -\frac{V_0}{\sqrt{4\pi}}$ [15,22], and, therefore, the modification due to the finite-range of the core-valence interaction is very small and this gives us confidence in using the zero-range approximation.

The effective two-body potential between the valence particle and core of the projectile $V_{vc}(r)$ can be approximated by the zero-range expression [15,21,22],

$$V_{vc}(r)\phi(\mathbf{r}, \mathbf{R}) = V_0\delta(\mathbf{r}) = -\frac{2\pi\hbar^2}{\mu_p}\sqrt{\frac{\alpha}{2\pi}}\delta(\mathbf{r}). \tag{17}$$

Equation (11) can then be written as

$$[T_{\mathbf{r}} - \Delta V_C(\mathbf{r}, \mathbf{R}) - \varepsilon_0 - \delta V(R)]\phi(\mathbf{r}, \mathbf{R}) = \frac{2\pi\hbar^2}{\mu_p}\sqrt{\frac{\alpha}{2\pi}}\delta(\mathbf{r}), \tag{18}$$

in which $\phi(\mathbf{r}, \mathbf{R}) \xrightarrow{r\to 0} \propto (\frac{1}{r} - \alpha)$ [23] and then obeys the usual condition [16,23],

$$\lim_{r\to 0}\frac{\partial}{\partial r}\ln[r\phi(\mathbf{r}, \mathbf{R})] = -\alpha. \tag{19}$$

The possibility of projectile breakup means that $\phi(\mathbf{r}, \mathbf{R})$ describes the (quasi) stationary state of the projectile while moving along the Rutherford trajectory.

We now transform from $(\mathbf{r}, \mathbf{R})$ to $(\mathbf{r}_c, R)$ coordinates,

$$\begin{aligned} \mathbf{r} &= \frac{m_c}{\mu_p}(\mathbf{R} - \mathbf{r}_c), \quad \delta(\mathbf{r}) = \left(\frac{m_c}{\mu_p}\right)^{-3}\delta(\mathbf{R} - \mathbf{r}_c), \\ \Delta_{\mathbf{r}} &= \left(\frac{m_c}{\mu_p}\right)^{-2}\Delta_{\mathbf{r}_c}, \quad T_{\mathbf{r}} = \frac{\mu_p}{m_c}\frac{-\hbar^2}{2m_c}\Delta_{\mathbf{r}_c} = \frac{\mu_p}{m_c}T_{\mathbf{r}_c}, \end{aligned} \tag{20}$$

and then Eq. (18) can be written as

$$\left(\frac{\mu_p}{m_c}T_{\mathbf{r}_c} + V_C(\mathbf{r}_c) - [V_C(\mathbf{R}) + \varepsilon_0 + \delta V(R)]\right)\phi(\mathbf{r}_c, R) = \frac{2\pi\hbar^2}{\mu_p}\sqrt{\frac{\alpha}{2\pi}}\left(\frac{m_c}{\mu_p}\right)^{-3}\delta(\mathbf{R}-\mathbf{r}_c). \tag{21}$$

Let us introduce

$$E_c(\mathbf{R}) = \frac{m_c}{\mu_p}[V_C(\mathbf{R}) + \varepsilon_0 + \delta V(R)] = \frac{\hbar^2 k^2}{2m_c}, \tag{22}$$

which denotes the energy of the projectile moving in the Coulomb potential $V_C(\mathbf{r}_c)$, and k is the wave number of the charged core in the field of the target. Equation (21) then becomes

$$\left(T_{\mathbf{r}_c} + \frac{m_c}{\mu_p}V_C(\mathbf{r}_c) - E_c\right)\frac{m_c}{\mu_p}\frac{m_c}{2\pi\hbar^2}\sqrt{\frac{2\pi}{\alpha}}\phi(\mathbf{r}_c, R) = \delta(\mathbf{R}-\mathbf{r}_c). \tag{23}$$

Taking the usual expression for the Coulomb potential,

$$V_C(\mathbf{r}_c) = \frac{Z_p Z_T e^2}{r_c}, \tag{24}$$

it is easy to show that the Coulomb Green's function $G_C[E_c(\mathbf{R}); \mathbf{r}_c, R]$ is the solution of Eq. (23) in which

$$G_C[E_c(\mathbf{R}); \mathbf{r}_c, R] = \frac{m_c}{\mu_p}\frac{m_c}{2\pi\hbar^2}\sqrt{\frac{2\pi}{\alpha}}\phi(\mathbf{r}_c, R), \tag{25}$$

which can be written as [24]

$$G_C[E_c(\mathbf{R}); \mathbf{r}_c, R] = \frac{2\mu_p}{\hbar^2}\frac{\Gamma(1+i\eta)}{2\pi i|\mathbf{R}-\mathbf{r}_c|}\left[\frac{\partial}{\partial\rho_+} - \frac{\partial}{\partial\rho_-}\right] \times W_{-i\eta,1/2}(-2i\rho_+)M_{-i\eta,1/2}(-2i\rho_-), \tag{26}$$

where $W_{-i\eta,1/2}$ and $M_{-i\eta,1/2}$ are the Whittaker functions, Γ is the γ function, $\eta = (\frac{m_c^2}{\mu_p})Z_p Z_T e^2/\hbar^2 k(R)$ denotes the Sommerfeld parameter and

$$\rho_\pm = \frac{1}{2}k(R)(\mathbf{R} + \mathbf{r}_c \pm |\mathbf{R}-\mathbf{r}_c|) = \frac{1}{2}k(R)\left(\mathbf{R} + \mathbf{r}_c \pm \frac{\mu_p}{m_c}|\mathbf{r}|\right), \tag{27}$$

in which $\lim_{r\to 0}\rho_\pm = \rho = k(R)R$.

By using the relations between Whittaker functions and Coulomb functions (F_l and $H_l^+ = G_l + iF_l$) [25,26],

$$\begin{aligned} F_l(\eta,\rho) &= C_l(\eta)2^{-l-1}(\mp i)^{l+1}M_{\pm i\eta,l+1/2}(\pm 2i\rho),\\ H_l^+(\eta,\rho) &= (-i)^l e^{(\pi\eta/2)+i\sigma_l(\eta)}W_{-i\eta,l+1/2}(-2i\rho),\\ C_l(\eta) &= \frac{2^l e^{-\pi\eta/2}|\Gamma(l+1+i\eta)|}{(2l+1)!},\\ \sigma_l(\eta) &= \mathrm{Ph}\,\Gamma(l+1+i\eta), \end{aligned} \tag{28}$$

we can obtain

$$G_C[E_c(\mathbf{R}); \mathbf{r}_c, R] = \frac{2\mu_p}{\hbar^2}\frac{1}{4\pi|\mathbf{R}-\mathbf{r}_c|}\left[\frac{\partial}{\partial\rho_+} - \frac{\partial}{\partial\rho_-}\right] \times H_0^+(\rho_+)F_0(\rho_-), \tag{29}$$

where $H_0^+ = G_0 + iF_0$, F_0, and G_0 are the regular and irregular Coulomb wave functions.

From Eq. (27),

$$\frac{\partial}{\partial r} = \frac{\mu_p k}{2m_c}\left(\frac{\partial}{\partial\rho_+} - \frac{\partial}{\partial\rho_-}\right). \tag{30}$$

Now, by applying the condition (19) by taking the limit $r \to 0$ and by using the properties of the Coulomb functions,

$$\begin{aligned} H_0^{+''}(\rho) &= \left(\frac{2\eta}{\rho} - 1\right)H_0^+(\rho),\\ F_0''(\rho) &= \left(\frac{2\eta}{\rho} - 1\right)F_0(\rho),\\ F_0G_0' - F_0'G_0 &= 1, \end{aligned} \tag{31}$$

one can obtain [6,16]

$$\frac{\mu_p}{m_c}k(R)\left\{H_0^{+'}(\rho)F_0'(\rho) - \left(\frac{2\eta}{\rho} - 1\right)H_0^+(\rho)F_0(\rho)\right\} = -\alpha, \tag{32}$$

where

$$k(R) = \sqrt{\frac{2m_c^2}{\mu_p\hbar^2}[V_C(R) + \varepsilon_0 + \delta V(R)]}, \tag{33}$$

$$\left(\frac{2\eta}{\rho} - 1\right) = \frac{2\left(\frac{m_c^2}{\mu_p}\right)Z_p Z_T e^2}{\hbar^2 k^2(R)R} - 1 = \frac{V_C(R)}{V_C(R) + \varepsilon_0 + \delta V(R)} - 1, \tag{34}$$

and we get

$$H_0^{+'}(\rho)F_0'(\rho) + \frac{\varepsilon_0 + \delta V(R)}{V_C(R) + \varepsilon_0 + \delta V(R)}H_0^+(\rho)F_0(\rho) = \frac{m_c}{\mu_p}\frac{-\alpha}{\sqrt{\frac{2m_c^2}{\mu_p\hbar^2}[V_C(R) + \varepsilon_0 + \delta V(R)]}} = -\sqrt{\frac{-\varepsilon_0}{[V_C(R) + \varepsilon_0 + \delta V(R)]}}. \tag{35}$$

By multiplying by $[V_C(R) + \varepsilon_0 + \delta V(R)]/\varepsilon_0$ and introducing the quantity $Q(R)$,

$$Q(R) = \sqrt{\frac{V_C(R) + \varepsilon_0 + \delta V(R)}{-\varepsilon_0}} = \frac{\mu_p}{m_c}\frac{k(R)}{\alpha}, \tag{36}$$

we obtain

$$\left(1 + \frac{\delta V(R)}{\varepsilon_0}\right)H_0^+(\rho)F_0(\rho) - Q^2(R)H_0^{+'}(\rho)F_0'(\rho) = Q(R). \tag{37}$$

$\delta V(R)$ is very small compared with the Coulomb potential at all distances, so this equation can be solved by assuming

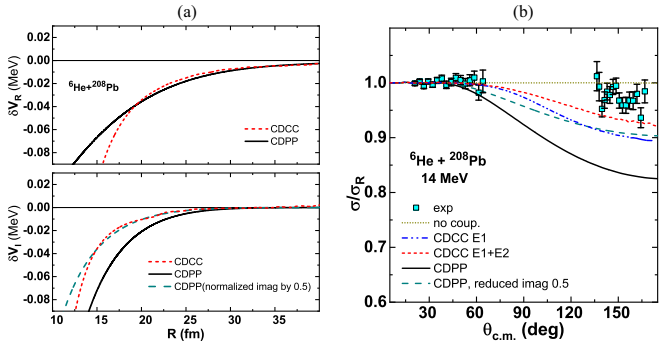

FIG. 2. (a) The real and imaginary CDPP for $^6\mathrm{He}+^{208}\mathrm{Pb}$ at 14 MeV compared with the TELP extracted from a CDCC calculation. (b) Angular distribution of $^6\mathrm{He}+^{208}\mathrm{Pb}$ elastic scattering at 14 MeV calculated with CDCC and the optical model using the CDPP compared with the data of Ref. [27].

$\delta V(R) \ll V_C(R)$ such that

$$Q(R) \approx \sqrt{\frac{V_C(R)+\varepsilon_0}{-\varepsilon_0}} = \sqrt{\frac{Z_p Z_T e^2}{-\varepsilon_0 R} - 1}. \tag{38}$$

By taking the real and imaginary parts of the quantities in Eq. (37) the CDPP $\delta V(R)$ can be written as

$$\delta V_R(R) = \varepsilon_0 \left[\frac{QG_0F_0 + Q^2G_0F_0G_0'F_0' + Q^2F_0^2F_0'^2}{F_0^4 + G_0^2F_0^2} - 1 \right]$$
$$\delta V_I(R) = \varepsilon_0 \left[\frac{Q^2F_0F_0' - QF_0^2}{F_0^4 + G_0^2F_0^2} \right]. \tag{39}$$

The root-mean-square (rms) radii of the real and imaginary parts of the CDPP are given by

$$R(\delta V_{R(I)}) = \langle R^2 \rangle_{R(I)}^{1/2} = \frac{\int dr\ 4\pi R^4 \delta V_{R(I)}(R)}{\int dr\ 4\pi R^2 \delta V_{R(I)}(R)}. \tag{40}$$

B. Application to $^6\mathrm{He}+^{208}\mathrm{Pb}$ at 14 MeV

In order to check how well the CDPP derived from Eq. (39) is able to describe experimental data, we investigated the $^6\mathrm{He}+^{208}\mathrm{Pb}$ elastic scattering measured at an incident energy of 14 MeV, well below the Coulomb barrier [27]. The CDPP was calculated for this system [solid curves in Fig. 2(a)] and included in an optical model (OM) calculation where the OM potential consisted of the standard Coulomb central potential plus the CDPP with no nuclear interaction. CDCC calculations, including only $E1$ excitations to the continuum, were also performed. The CDCC calculations employed the dineutron model of ^{6}He [28]. This model reproduces reasonably well the $B(E1)$ transition strength for the ^{6}He. Thus, the CDPP extracted from these calculations by means of the trivially equivalent method [8], the so-called TELP (trivially equivalent local potential), should serve as a realistic test of the method presented in this paper.

In Fig. 2(a) we compare the CDPP calculated using Eq. (39), the solid curves, with the TELP extracted from the CDCC calculations, the dashed curves. The real part of the CDPP coincides very well with the real part of the TELP for projectile-target separations larger than 20 fm whereas the imaginary part is more absorptive. This means that the reaction cross section (essentially the ^{6}He Coulomb breakup cross section in this context) of the CDCC calculation will be smaller than the OM result obtained using the CDPP since this quantity depends mostly on the imaginary part of the potential, whereas the dipole polarizability of ^{6}He, which depends solely on the real part, should be correctly represented by the CDPP calculated using Eq. (39).

The problem of the large imaginary part of the CDPP is well illustrated when the model calculations are compared with the data for $^6\mathrm{He}+^{208}\mathrm{Pb}$ elastic scattering, see Fig. 2(b). Both models underpredict the measured cross sections at backward angles, the OM calculation using the CDPP significantly more so than the CDCC calculation due to the stronger imaginary potential. In the case of the CDCC calculations the underprediction can be partly accounted for by including $E2$ excitations in addition to the $E1$ as demonstrated in Ref. [29] and discussed in Ref. [27]. A comparison of the curves in Fig. 2(b) labeled "CDCC $E1$" and "CDCC $E1+E2$" shows the size of the effect in this case. Also plotted in Fig. 2(b) is the result of an OM calculation where the imaginary part of the CDPP was multiplied by a factor of 0.5 to match the imaginary part of the TELP obtained from the CDCC calculation, see Fig. 2(a). It matches the CDCC $E1$' result rather closely, confirming that the real part of the CDPP realistically reflects the dipole polarizability. Since the imaginary part of the CDPP is produced by the breakup, these comparisons suggest that the too large absorption of the CDPP is partly due to the omission of the $E2$ couplings and partly due to the simplifications inherent in the handling of the $E1$ breakup effects, for example, the condition on the internal wave-function (19) which assumes the limit as a real value only.

To summarize, the real part of the CDPP derived in this paper compares well with that generated by the CDCC calculation and is used in the next section to obtain the dipole polarizability.

C. Dipole polarizability from the CDPP

If the long-range attractive part of the CDPP (39) is fitted by the classical expression (2), one can obtain a value for the dipole polarizability α_0. At large R (larger than the rms radius) $\rho = kR$ is also large, thus, F_0 and F_0' are much smaller than G_0 and G_0', and Eq. (39) may be approximated as

$$\delta V_R(R) \approx \varepsilon_0 \left[\frac{Q + Q^2G_0'F_0'}{G_0F_0} - 1 \right],$$
$$\delta V_I(R) \approx \varepsilon_0 \left[\frac{Q^2F_0' - QF_0}{G_0^2F_0} \right]. \tag{41}$$

Introducing this into Eq. (2) we obtain the following result for what we will term the polarizability function $\alpha_0(R)$:

$$\alpha_0(R) = \frac{-2\varepsilon_0 R^4}{Z_T^2 e^2} \delta V_R(R)$$
$$= \frac{-2\varepsilon_0 R^4}{Z_T^2 e^2} \frac{Q + Q^2G_0'F_0' - G_0F_0}{G_0F_0}. \tag{42}$$

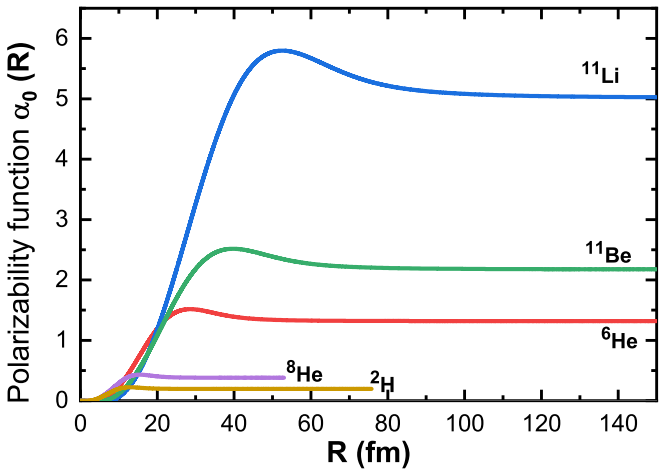

FIG. 3. The polarizability functions $\alpha_0(R)$ for ^{2}H, ^{6}He, ^{8}He, ^{11}Li, and ^{11}Be + ^{208}Pb at energies near the Coulomb barrier, calculated using Eq. (44). $\alpha_0^{\max} = 0.43, 1.5, 0.22, 5.76, 2.5$ fm^3 located at 15.5, 28.6, 12.9, 52.4, 39.7 fm for ^{2}H, ^{6}He, ^{8}He, ^{11}Li, and ^{11}Be, respectively.

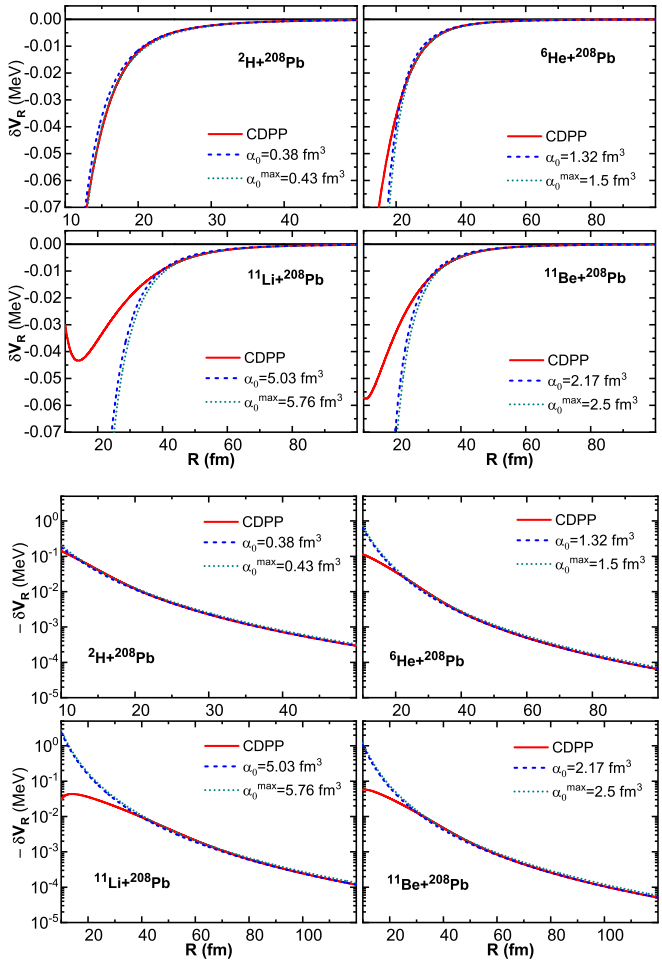

FIG. 4. CDPPs for ^{2}H, ^{6}He, ^{11}Li, and ^{11}Be + ^{208}Pb on linear and logarithmic scales. The solid lines denote the real CDPP calculated in this paper [Eq. (39)] and the dashed lines represent the CDPP calculated using the semiclassical formula (2) with α_0 tuned to give the best match to our CDPP.

TABLE I. The dipole polarizability α_0 (in fm^3) of weakly bound light nuclei extracted from the fitting of the CDPP to the classical expression (as in Fig. 4) using Eq. (44). The separation energies (ε_0, in MeV) are taken from the recent atomic mass evaluation [30].

Projectile	Configuration	$-\varepsilon_0$	$\alpha_0^{\max}$	R_0	Fitted α_0
^{2}H	^{1}H + n	2.225	0.428	15.45	0.375
^{6}He	^{4}He + 2n	0.975	1.505	28.55	1.316
^{6}He	^{5}He + 1n	1.710	0.196	14.95	0.171
^{7}He	^{5}He + 2n	1.301	0.580	20.95	0.508
^{8}He	^{4}He + 4n	3.10	0.223	12.90	0.195
^{8}He	^{6}He + 2n	2.125	0.159	13.35	0.139
^{8}He	^{7}He + n	2.535	0.048	9.55	0.042
^{9}He	^{7}He + 2n	1.280	0.334	18.45	0.291
^{6}Li	^{5}Li + n	5.660	0.040	7.45	0.035
^{7}Li	^{6}Li + n	7.251	0.018	5.70	0.015
^{8}Li	^{7}Li + n	2.033	0.167	13.95	0.146
^{9}Li	^{8}Li + n	4.062	0.033	7.75	0.028
^{10}Li	^{8}Li + 2n	4.036	0.059	9.00	0.052
^{11}Li	^{9}Li + 2n	0.369	5.766	52.40	5.026
^{11}Li	^{10}Li + n	0.396	2.254	40.90	1.964
^{12}Li	^{10}Li + 2n	0.190	17.96	82.70	15.64
^{13}Li	^{12}Li + n	0.100	24.96	106.1	21.90
^{9}Be	^{8}Be + n	1.665	0.346	17.75	0.302
^{10}Be	^{9}Be + n	6.812	0.017	5.80	0.014
^{11}Be	^{10}Be + n	0.502	2.498	39.65	2.173
^{12}Be	^{11}Be + n	3.171	0.052	9.40	0.045
^{12}Be	^{10}Be + 2n	3.672	0.085	10.20	0.074
^{13}Be	^{11}Be + 2n	2.661	0.136	12.45	0.119
^{14}Be	^{13}Be + n	1.780	0.120	13.45	0.104
^{14}Be	^{12}Be + 2n	1.270	0.510	21.00	0.444
^{16}Be	^{15}Be + n	0.450	1.424	35.55	1.240
^{12}B	^{11}B + n	3.370	0.072	10.10	0.063
^{14}B	^{13}B + n	0.970	0.631	23.85	0.550
^{15}B	^{14}B + n	2.778	0.067	10.40	0.058
^{16}B	^{14}B + 2n	2.690	0.133	12.45	0.116
^{17}B	^{16}B + n	1.470	0.184	15.80	0.160
^{17}B	^{15}B + 2n	1.380	0.445	19.95	0.388
^{18}B	^{16}B + 2n	1.460	0.352	18.55	0.307
^{19}B	^{18}B + n	0.090	39.07	122.5	34.09
^{19}B	^{17}B + 2n	0.090	82.72	147.4	72.01
^{15}C	^{14}C + n	1.218	0.500	21.30	0.435
^{17}C	^{16}C + n	0.734	1.063	29.25	0.925
^{19}C	^{18}C + n	0.580	1.354	33.00	1.178
^{22}C	^{21}C + n	0.100	33.74	115.1	29.36
^{22}C	^{20}C + 2n	0.035	578.47	304.6	503.27
^{18}N	^{17}N + n	2.828	0.087	11.10	0.075
^{20}N	^{19}N + n	2.160	0.120	12.90	0.104
^{22}N	^{21}N + n	1.540	0.193	15.90	0.169
^{23}O	^{22}O + n	2.730	0.073	10.80	0.064
^{26}O	^{25}O + n	0.739	0.780	27.15	0.679
^{26}F	^{25}F + n	0.730	1.012	29.10	0.881
^{27}F	^{26}F + n	1.610	0.193	15.70	0.168
^{27}F	^{25}F + 2n	2.340	0.190	14.25	0.165
^{28}F	^{26}F + 2n	1.410	0.484	20.45	0.422
^{29}F	^{28}F + n	1.320	0.248	17.65	0.216
^{29}F	^{27}F + 2n	1.130	0.701	23.75	0.610
^{27}Ne	^{26}Ne + n	1.500	0.274	17.50	0.238
^{29}Ne	^{28}Ne + n	0.970	0.567	23.45	0.493
^{31}Ne	^{30}Ne + n	0.170	16.12	83.90	14.02
^{34}Na	^{33}Na + n	0.170	16.16	84.00	14.06

TABLE I. (*Continued.*)

Projectile	Configuration	$-\varepsilon_0$	$\alpha_0^{\max}$	R_0	Fitted α_0
^{35}Mg	^{34}Mg $+n$	0.750	0.932	28.35	0.811
^{37}Mg	^{36}Mg $+n$	0.240	8.130	64.95	7.083

The function $\alpha_0(R)$ reaches a maximum value ($\alpha_0^{\max}$) at a definite distance R_0,

$$\alpha_0^{\max} = \max[\alpha_0(R)] = \max\left[\frac{-2\varepsilon_0 R^4}{Z_T^2 e^2}\frac{Q+Q^2G_0'F_0'-G_0F_0}{G_0F_0}\right]. \quad (43)$$

The function $\alpha_0(R)$ completely saturates [$[d\alpha_0(R)/dR \approx 0]$ at large distances $R > 2R_0$ as shown in Fig. 3. At these distances the CDPP (39) is proportional to $1/R^4$ and matches exactly the classical formula (2). One may then extract the electric dipole polarizability as follows:

$$\alpha_0 \approx \alpha_0(R > 2R_0) \text{ at which } \frac{d\alpha_0(R)}{dR} \approx 0, \quad (44)$$

thus obviating the need for the fitting procedure. Figure 4 presents our real CDPP from Eq. (39) compared to the fitted classical expression for four different systems, ^{2}H + ^{208}Pb, ^{6}He + ^{208}Pb, ^{11}Li + ^{208}Pb, and ^{11}Be + ^{208}Pb. We compare fits to the CDPP with both $\alpha_0^{\max}$ and α_0. It is clear that α_0 fits the CDPP well at large distances whereas $\alpha_0^{\max}$ fits it only at distances around R_0.

III. APPLICATION TO WEAKLY BOUND LIGHT EXOTIC NUCLEI

As discussed in Sec. II C, the dipole polarizability can be determined by fitting the calculated CDPP with the classical formula using Eq. (44). The results obtained for many weakly bound and neutron-rich nuclei are listed in Table I.

It should be recalled that the CDPP derived in this paper is predicated upon a two-body deuteronlike structure of the projectile (i.e., a charged core plus a neutron or cluster of neutrons). In producing Table I it has, therefore, been necessary to assume a cluster structure of this type for the nuclei considered. In some cases this will not cover the most favored or likely clustering configuration, or there may be more than one equally likely configuration of this type. We thus do not necessarily advocate these configurations as being the most physically realistic, but we give the values of α_0 obtained under the various clustering assumptions in order to obtain a systematic of the variation of α_0 with different physical parameters and, in the case of some of the more exotic nuclei considered, as a potential aid in probing possible cluster structures. In Table II we compare our results for α_0 (mean value of the two methods from Table I) with values from the literature for nuclei which are known to exhibit pronounced deuteronlike clustering. We also compare with polarizability values extracted from the available $dB(E1,\varepsilon)/d\varepsilon$ data using Eq. (1). These cases provide a realistic test of the current procedure for determining α_0, and our results are in good agreement with the previous studies.

Table I shows a considerable variation of α_0 for a given nucleus according to the assumed cluster configuration. For nuclei with well-known dominant configurations these support our results. For example, in the case of ^{6}He we see from Table I that the α_0 value for the ^{4}He $+2n$ configuration is much larger than for an assumed ^{5}He $+n$ structure, in agreement with the known $2n$ halo nature of this nucleus. The same applies to the ^{9}Li $+2n$ and ^{10}Li $+n$ configurations of ^{11}Li. We also note that for some of the more exotic nuclei we predict large values of α_0 for certain configurations which it would be of interest to confirm experimentally. In particular, if a ^{20}C $+2n$ cluster configuration is assumed for the exotic carbon isotope ^{22}C, the predicted value of α_0 is truly enormous at about 500 fm^3. Although we do not claim that this value is completely realistic, particularly in light of the uncertainty in the S_{2n} value for ^{22}C (see below), it strongly suggests that if this nucleus does indeed exhibit a $2n$ halo structure a measurement of its near-barrier elastic scattering from a heavy target such as ^{208}Pb would prove interesting.

Figure 5 plots the average dependence of the polarizability, taken from Table I, on the threshold energy for a wide range of nuclei. It is clear that the polarizability value depends inversely on the square of the threshold energy.

It was found from Table I that the dipole polarizability α_0 is about 0.87 ($\approx\sqrt{2}\pi^2/16$) of $\alpha_0^{\max}$ so we redefine the dipole polarizability as

$$\alpha_0 \approx \frac{\sqrt{2}\pi^2}{16}\max[\alpha_0(R)] \approx \max\left[\frac{-2\sqrt{2}\pi^2}{16}\frac{\varepsilon_0 R^4}{Z_T^2 e^2}\left(\frac{Q+Q^2G_0'F_0'-G_0F_0}{G_0F_0}\right)\right]. \quad (45)$$

Also, by fitting the values from Table I and other values for all possible configurations for these projectiles the following

TABLE II. Comparison between our values for the dipole polarizability α_0 (in fm^3) and values from the literature for selected nuclei.

Projectile	Configuration	$-\varepsilon_0$	Dipole polarizability α_0	
		MeV	Our paper	Previous
^{2}H	^{1}H $+n$	2.225	0.38	0.32 [31], 0.42,0.62 [14], 0.56 [32,33], 0.7 [5]
^{6}He	^{4}He $+2n$	0.975	1.32	1.00 ± 14 [46], 1.2 [34], 1.3 [35], 1.88 [36], 1.99 ± 40 [37], 1.07[a] [9]
^{11}Li	^{9}Li $+2n$	0.369	5.03	5.7 [35], 5.18[a] [11]
^{11}Be	^{10}Be $+n$	0.502	2.17	2.5 [38], 2.6[a] [10]

[a]From Eq. (1).

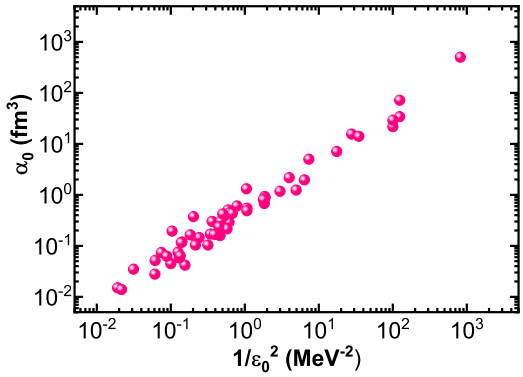

FIG. 5. The dependence of the dipole polarizability on ε_0 for different weakly bound light nuclei taken from Table I.

expression was obtained:

$$\alpha_0^{\max} = \frac{1}{\sqrt{2}\pi^2}\frac{\hbar^2}{\mu_p}\left(\frac{N_v Z_p e}{A_p}\right)^2 \frac{1}{\varepsilon_0^2} = \frac{1}{\sqrt{2}\pi^2}\frac{\hbar^2\mu_p}{m_c^2}\frac{(Z_p e)^2}{\varepsilon_0^2}, \tag{46}$$

where N_v is the number of neutrons in the valence cluster of the projectile. So that we may write

$$\alpha_0 = \frac{\sqrt{2}\pi^2}{16}\alpha_0^{\max} = \frac{1}{16}\frac{\hbar^2}{\mu_p}\left(\frac{N_v Z_p e}{A_p}\right)^2 \frac{1}{\varepsilon_0^2}, \tag{47}$$

which is the formula given in Ref. [47]. The same expression may also be extracted by applying Eq. (1) for $dB(E1,\varepsilon)/d\varepsilon$ given in Ref. [48],

$$\frac{dB(E1,\varepsilon)}{d\varepsilon} = \frac{3\hbar^2}{\pi^2\mu}\left(\frac{N_v Z_p e}{A_p}\right)^2 \frac{\sqrt{\varepsilon_0}(\varepsilon-\varepsilon_0)^{3/2}}{\varepsilon^4}, \tag{48}$$

so that

$$\alpha_0 = \frac{8\pi}{9}\int_{\varepsilon_0}^{\infty}\frac{1}{\varepsilon}\frac{dB(E1,\varepsilon)}{d\varepsilon}d\varepsilon = \frac{1}{16}\frac{\hbar^2}{\mu_p}\left(\frac{N_v Z_p e}{A_p}\right)^2 \frac{1}{\varepsilon_0^2}. \tag{49}$$

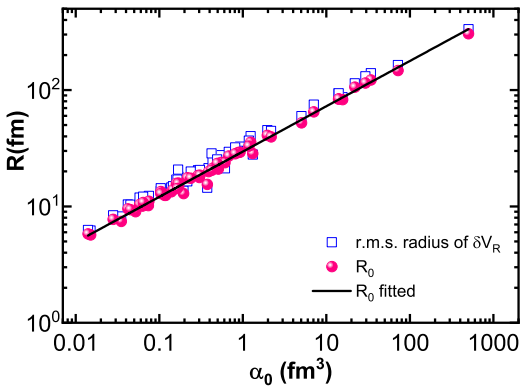

FIG. 6. The dependence of the root-mean-square radius of the real part of the CDPP and R_0 on the dipole polarizability for different weakly bound light nuclei considered in Table I.

TABLE III. Calculated dipole polarizability values for ^{11}Be (as ^{10}Be $+n$) incident on different targets.

Target	$\alpha_0^{\max}$	R_0	Fitted α_0 [Eq. (44)]
^{1}H	2.441	3.75	2.155
^{4}He	2.456	5.55	2.164
^{12}C	2.475	10.15	2.168
^{64}Zn	2.490	23.65	2.172
^{120}Sn	2.492	30.75	2.172
^{208}Pb	2.495	39.65	2.173

This gives us confidence that our expression for the CDPP yields the correct dipole polarizability. Furthermore, the quadrupole and octupole polarizabilities could also be extracted from the CDPP, although we leave this for future work.

Closer inspection of Table I reveals a dependence of the root-mean-square radius of the real part of the CDPP, Eq. (40), and R_0 on the dipole polarizability. This dependence is shown in Fig. 6. There is a clear linear relation between the logarithm of α_0 and these radii. R_0 is now easily given by $R_0 = 28.05(\alpha_0^{\max})^{0.389} = 29.58(\alpha_0)^{0.389}$, and $R(\delta V_{R(I)}) = 30.83(\alpha_0^{\max})^{0.392} = 32.51(\alpha_0)^{0.392}$. Thus, we have another method for determining the polarizability from the real part of the CDPP.

The methods presented here for the determination of the dipole polarizability from the real part of the CDPP are independent of the target. We have calculated the dipole polarizability according to Eq. (44) and by fitting the real parts of the CDPPs for ^{11}Be scattered from a range of target nuclei. The results are presented in Table III. Although the values of R_0 obviously vary, the polarizability values are not affected by the choice of target. For some exotic light nuclei the threshold energy is not well known. For example, for ^{11}Li there are many two-neutron separation energies derived from various mass measurements: CERN [39]; TOFI-LANL [40]; KEK [41]; MSU [42]; MISTRAL [43]; TITAN [44]. These are listed in Table IV. The real part of the CDPP and the dipole polarizability were calculated using these values to investigate the sensitivity of α_0 to the value of the two-neutron separation energy. The results are presented in Table IV. It is seen that the value of α_0 dramatically depends on the two-neutron separation energy and satisfies the expression (47). Note that

TABLE IV. The sensitivity of the dipole polarizability α_0 for ^{11}Li (with an assumed ^{9}Li $+2n$ configuration) extracted from the CDPP for the ^{11}Li $+$ ^{208}Pb system to different values of the $2n$ separation energy ε_0.

$\varepsilon_0 = S_{2n}$ (KeV)	Reference	$\alpha_0^{\max}$	R_0	Fitted α_0 [Eq. (44)]
170 ± 80	[39]	27.184	94.20	23.684
247 ± 80	[45]	12.872	71.00	11.218
295 ± 35	[42]	9.023	62.20	7.864
320 ± 120	[40]	7.668	58.45	6.683
340 ± 50	[41]	6.792	55.80	5.920
369 ± 65	[44]	5.756	52.40	5.018
378 ± 5	[43]	5.494	51.60	4.789

TABLE V. The sensitivity of ε_0 on dipole polarizability values of ^{11}Be + ^{208}Pb (as ^{10}Be + n with $\varepsilon_0 = -0.502$ MeV).

	$\alpha_0^{\max}$	R_0	Fitted α_0 [Eq. (44)]
$\varepsilon_0 - 10\% = 0.452$ MeV	3.077	42.90	2.680
$\varepsilon_0 = 0.502$ MeV	2.495	39.65	2.173
$\varepsilon_0 + 10\% = 0.552$ MeV	2.062	36.90	1.797

the most recent measurement of the separation energy (0.369 MeV) [44], used to calculate the value of α_0 for ^{11}Li in Table I, gives the result closest to the determination from $dB(E1,\varepsilon)/d\varepsilon$ data [11] by applying Eq. (1), see Table II.

A similar exercise was carried out for ^{11}Be (with an assumed ^{10}Be + n configuration), probing the effect of a hypothetical ±10% variation in ε_0 on the value of α_0 obtained. The results presented in Table V show a variation in α_0 of approximately ±20%, suggesting that calculations of α_0 might be useful as an additional constraint on binding energies for some of the more exotic neutron rich light nuclei.

IV. SUMMARY AND CONCLUSION

The dynamical polarization for weakly bound projectiles moving in the Coulomb field of a heavy target was analyzed and the related CDPP derived by solving the Schrödinger equation using the adiabatic approximation and a new expression for the CDPP presented in terms of separation energies and regular and irregular Coulomb functions. From a comparison of the real part of our CDPP with the classical formula we extract a new expression for the electric dipole polarizability (α_0). The α_0 values for a wide range of weakly bound nuclei were determined and compared with available experimental and theoretical values. Uncertainties in the separation energy (for example, the different values for ^{11}Li) affect strongly the calculated polarizability.

The present CDPP was applied to an optical model calculation of the sub-barrier elastic scattering of ^{6}He + ^{208}Pb and compared with a CDCC calculation. The real part of our CDPP was found to agree very well with the real part of the TELP DPP derived from the CDCC calculations, confirming the accuracy of the method for systems where Coulomb dipole excitation is dominant, although the imaginary part was too strong, leading to too great an absorption when used to calculate the sub-barrier elastic scattering.

Values of α_0 were calculated for several weakly bound neutron-rich exotic nuclei with various assumed clustering configurations. These values provide predictions for nuclei where the near-barrier elastic scattering from heavy targets should prove of interest, i.e., those with large α_0. The variation of α_0 as a function of the binding energy for different cluster configurations and of the binding energy itself for a given configuration for systems where the masses are not well known suggest that our method for calculating α_0 may provide a useful further constraint on the masses of some of the more exotic neutron-rich nuclei as well as an indication of which clustering mode or modes will be dominant in nuclei where several such possibilities exist.

ACKNOWLEDGMENTS

This work was funded by the Polish National Agency for Academic Exchange (NAWA) within the Ulam Programme under Grant Agreement No. PPN/ULM/2019/1/00189/U/00001. We are grateful to Prof. Takashi Nakamura and Prof. Thomas Aumann for providing us with $B(E1)$ distribution data.

[1] M. V. Andrés, J. Gómez-Camacho, and M. A. Nagarajan, Nucl. Phys. **A583**, 817 (1995); **A579**, 273 (1994); **A724**, 113 (2003).
[2] M. V. Andrés and J. Gómez-Camacho, Phys. Rev. Lett. **82**, 1387 (1999).
[3] A. M. Moro, J. A. Lay, and J. Gómez-Camacho, Phys. Lett. B **811**, 135959 (2020).
[4] B. J. Malenka, U. E. Kruse, and N. F. Ramsey, Phys. Rev. **91**, 1165 (1953).
[5] N. L. Rodning, L. D. Knutson, W. G. Lynch, and M. B. Tsang, Phys. Rev. Lett. **49**, 909 (1982).
[6] L. Borowska, K. Terenetsky, V. Verbitsky, and S. Fritzsche, Phys. Rev. C **76**, 034606 (2007).
[7] K. Alder and A. Winther, *Electromagnetic Excitation* (North-Holland, Amsterdam, 1975).
[8] M. A. Franey and P. J. Ellis, Phys. Rev. C **23**, 787 (1981).
[9] T. Aumann, D. Aleksandrov, L. Axelsson, T. Baumann, M. J. G. Borge, L. V. Chulkov *et al.*, Phys. Rev. C **59**, 1252 (1999).
[10] R. Palit, P. Adrich, T. Aumann, K. Boretzky, B. V. Carlson, D. Cortina *et al.*, Phys. Rev. C **68**, 034318 (2003).
[11] T. Nakamura, A. M. Vinodkumar, T. Sugimoto, N. Aoi, H. Baba, D. Bazin *et al.*, Phys. Rev. Lett. **96**, 252502 (2006).
[12] C. A. Bertulani and A. Gade, Phys. Rep. **485**, 195 (2010).
[13] J. Oppenheimer and M. Phillips, Phys. Rev. **48**, 500 (1935).
[14] C. F. Clement, Phys. Rev. **128**, 2724 (1962); **128**, 2728 (1962).
[15] G. Baur, F. Rösel, and D. Trautmann, Nucl. Phys. **A288**, 113 (1977).
[16] V. P. Verbitsky and K. O. Terenetsky, Yad. Fiz. **55**, 362 (1992) [Sov. J. Nucl. Phys. **55**, 198 (1992)].
[17] R. Shyam, P. Banerjee, and G. Baur, Nucl. Phys. **A540**, 341 (1992).
[18] Y. N. Demkov and V. N. Ostrovskii, *Zero-Range Potentials and their Applications in Atomic Physics* (Springer, New York, 1988).
[19] G. Baur, F. Rosel, D. Trautmann, and R. Shyam, Phys. Rep. **111**, 333 (1984).
[20] L. Hulthén and M. Sugawara, in *Handbuch der Physik*, edited by S. Flügge (Springer-Verlag, Berlin, 1957), Vo1. 39, p. 33.
[21] G. Baur and D. Trautmann, Nucl. Phys. **A191**, 321 (1972).
[22] G. Baur and D. Trautmann, Phys. Rep. **25**, 293 (1976).
[23] Y. N. Demkov and G. F. Drukarev, Zh. Éksp. Teor. Fiz. **47**, 918 (1964) [Sov. Phys. JETP **20**, 614 (1965)].
[24] L. Hostler and R. H. Pratt, Phys. Rev. Lett. **10**, 469 (1963).

[25] M. Abramowitz and I. A. Stegun, *Handbook of Mathematical Functions: With Formulas, Graphs, and Mathematical Tables*, Dover Books on Mathematics (Dover, New York, 1964).
[26] F. W. J. Olver, D. W. Lozier, R. F. Boisvert, and C. W. Clark, *NIST Handbook of Mathematical Functions*, 1st ed. (NIST, New York, 2010).
[27] A. M. Sánchez-Benítez *et al.*, Nucl. Phys. **A803**, 30 (2008).
[28] A. M. Moro, K. Rusek, J. M. Arias, J. Gómez-Camacho, and M. Rodríguez-Gallardo, Phys. Rev. C **75**, 064607 (2007).
[29] K. Rusek, I. Martel, J. Gómez-Camacho, A. M. Moro, and R. Raabe, Phys. Rev. C **72**, 037603 (2005).
[30] M. Wang, W. J. Huang, F. G. Kondev, G. Audi, S. Naimi, and X. Xu, Chin. Phys. C **45**, 030003 (2021).
[31] J. Sawicki, Acta Phys. Pol. **13**, 225 (1954).
[32] N. F. Ramsey, B. J. Malenka, and U. E. Kruse, Phys. Rev. **91**, 1162 (1953).
[33] B. W. Downs, Phys. Rev. **98**, 194 (1955).
[34] V. V. Parkar, I. Martel, A. M. Sánchez-Benítez, L. Acosta, K. Rusek, Ł. Standylo, and N. Keeley, Acta Phys. Pol., B **42**, 761 (2011).
[35] N. Keeley, K. W. Kemper, and K. Rusek, Phys. Rev. C **88**, 017602 (2013).
[36] J. A. Lay, A. M. Moro, J. M. Arias, and J. Gómez-Camacho, Phys. Rev. C **82**, 024605 (2010).
[37] K. Pachucki and A. M. Moro, Phys. Rev. A **75**, 032521 (2007).
[38] K. Rusek, I. Martel, A. M. Sánchez-Benítez, and L. Acosta, Acta Phys. Pol., B **43**, 233 (2012).
[39] C. Thibault *et al.*, Phys. Rev. C **12**, 644 (1975).
[40] J. M. Wouters, R. H. Kraus Jr., D. J. Vieira, G. W. Butler, and K. E. G. Löbner, Z. Phys. A **331**, 229 (1988).
[41] T. Kobayashi *et al.*, Report No. 91022, 1991 (unpublished).
[42] B. M. Young *et al.*, Phys. Rev. Lett. **71**, 4124 (1993).
[43] C. Bachelet, G. Audi, C. Gaulard, C. Guénaut, F. Herfurth, D. Lunney, M. de Saint Simon, and C. Thibault, Phys. Rev. Lett. **100**, 182501 (2008).
[44] M. Smith *et al.*, Phys. Rev. Lett. **101**, 202501 (2008).
[45] F. Ajzenberg Selove, Nucl. Phys. **A506**, 1 (1990).
[46] R. Goerke, S. Bacca, and N. Barnea, Phys. Rev. C **86**, 064316 (2012).
[47] V. F. Kharchenko, Int. J. Mod. Phys. E **22**, 1350031 (2013).
[48] C. A. Bertulani and A. Sustich, Phys. Rev. C **46**, 2340 (1992).